

Supplementary Information

Solvent-solute cooperative mechanism for symmetry-breaking charge transfer

Changmin Lee,^a Cheol Ho Choi,^{*b} and Taiha Joo^{*a}

^aDepartment of Chemistry, Pohang University of Science and Technology (POSTECH), Pohang 37673, South Korea, e-mail: thjoo@postech.ac.kr

^bDepartment of Chemistry, Kyungpook National University, Daegu 41566, South Korea, e-mail: cchoi@knu.ac.kr

Table of Contents

Fig. S1 Absorption and fluorescence spectra of bianthracene in various solvents.

Fig. S2 Absorption and fluorescence spectra of anthracene in heptane.

Fig. S3 Excitation spectra of bianthracene in acetonitrile.

Fig. S4 TF spectra of bianthracene in heptane.

Fig. S5 TF spectra of bianthracene in acetone.

Fig. S6 Global fitting results of the TF spectra of bianthracene in acetonitrile.

Fig. S7 Time-resolved spectra of pure solvents acetonitrile and ethanol.

Fig. S8 Integrated area of the whole TF spectral region.

Fig. S9 Equilibration of the ground state in MD simulation.

Fig. S10 Oscillator strength of the S_2 state of representative MD simulation points.

Table S1 & S2 Transition amplitudes from MD simulation result.

Fig. S11 Molecular orbitals from MD simulation result.

Fig. S12 Ensemble averaged dipole moments of the S_1 state and transition energy between the ground and S_1 state from all MD simulations.

Fig. S13 Radial distribution function in the course of MD simulation.

Fig. S14 Spatial distribution of solvent molecules contributing to the electric field.

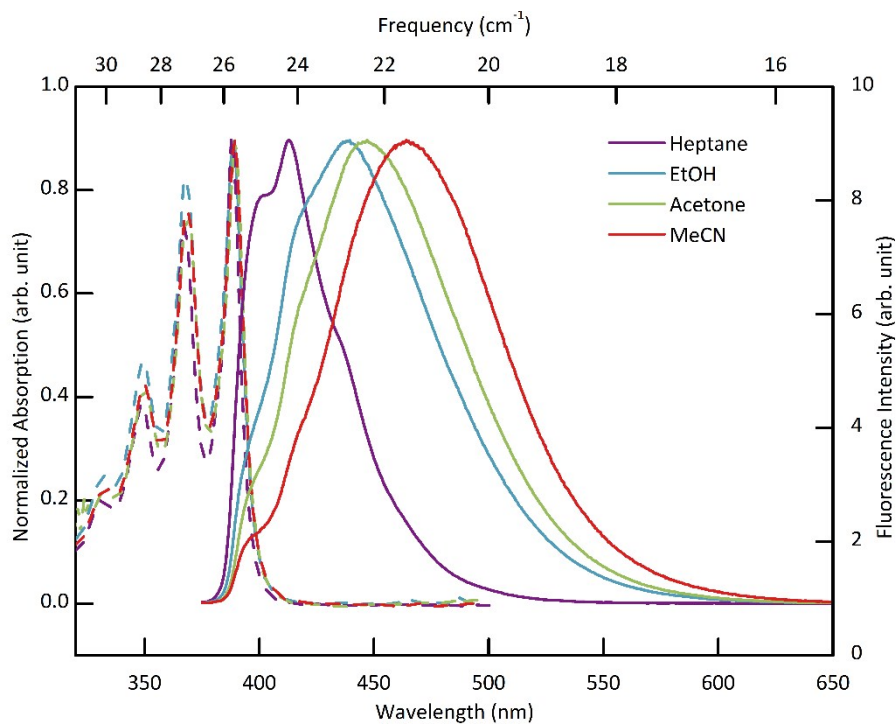


Fig. S1 Absorption and fluorescence spectra of BA in various solvents. The absorption spectra are almost the same in all solvents. Dashed lines are absorption and solid lines are fluorescence spectra. Only the LE fluorescence is apparent in nonpolar solvent heptane, whereas dual fluorescence from both LE and CT states are evident in polar solvents. Stokes shift increases as the solvent polarity increases demonstrating that the long wavelength band arises from the CT state.

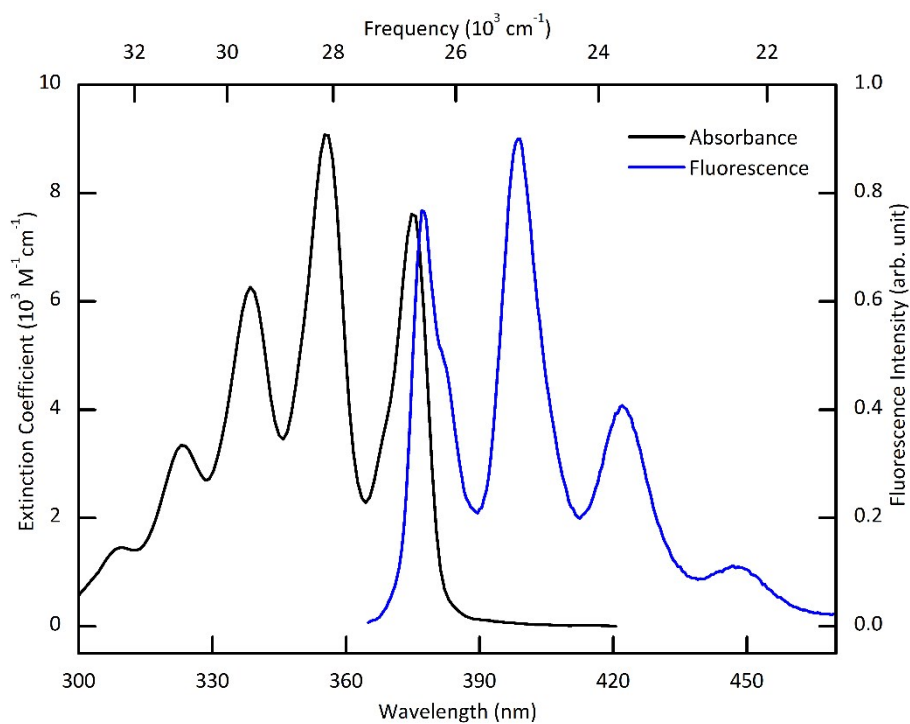


Fig. S2 Absorption and Fluorescence Spectra of anthracene in heptane. Band structure of the absorption spectrum is similar to that of BA, and the absorption and fluorescence spectra display good mirror symmetry, which indicates indirectly that the fluorescence of BA in polar solvents is a result of strong coupling between the two anthracene rings.

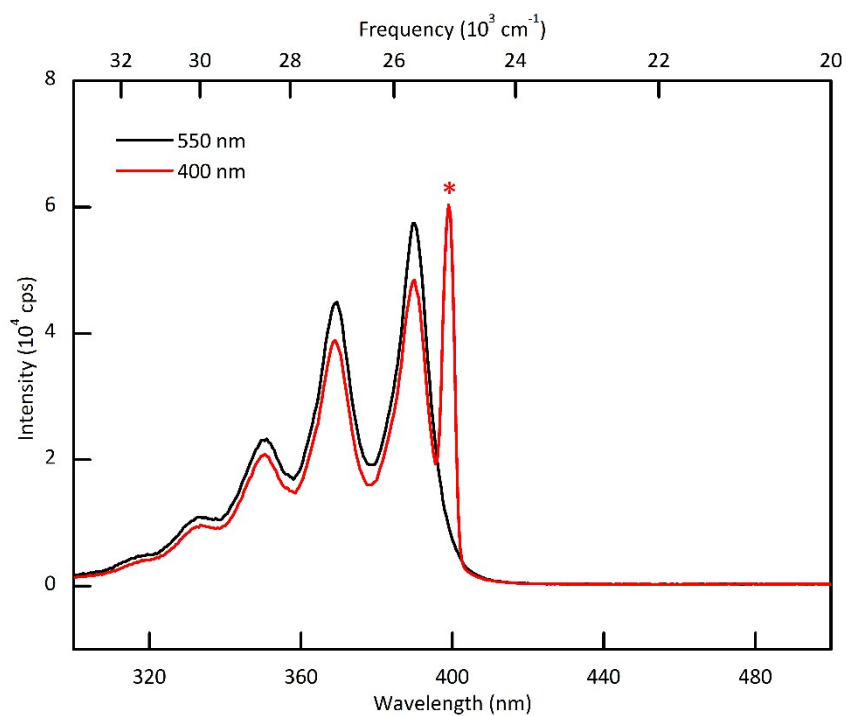


Fig. S3 Excitation spectra of BA in acetonitrile. The detection wavelengths are 550 nm (black) and 400 nm (red), which are the blue and red sides of fluorescence spectrum. The spectra are almost the same indicating that they originated from the same state. There is no direct CT excitation state even in the longer wavelength up to 500 nm. The * peak at 400 nm is from the light source.

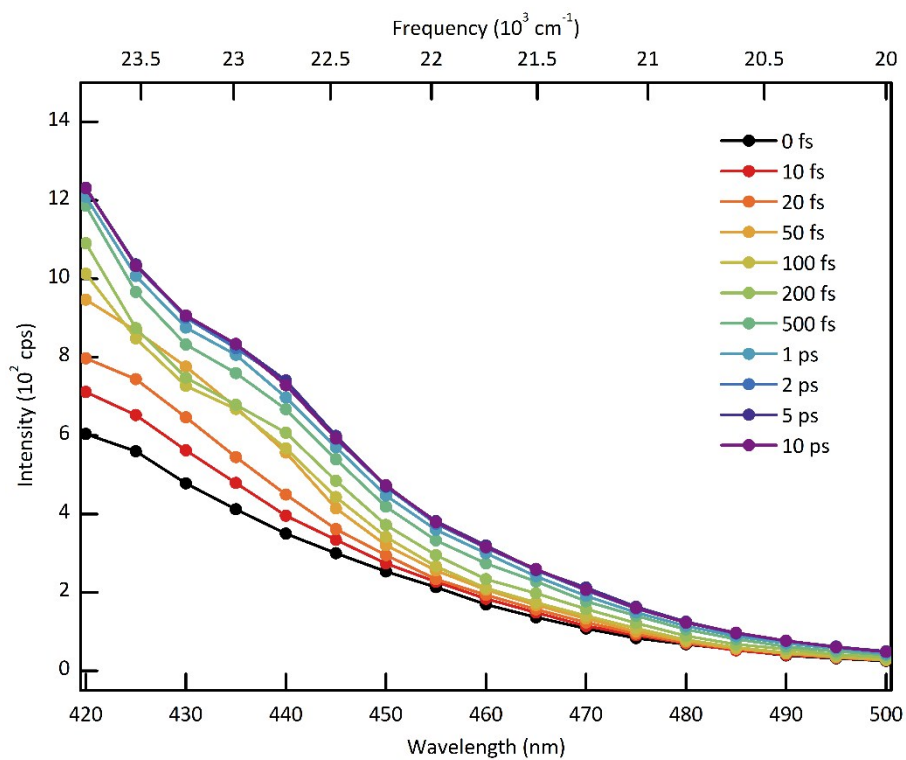


Fig. S4 TF spectra of BA in heptane at the given time delays. Because heptane is nonpolar, SBCT reaction does not take place, that is, the fluorescence arises from the LE state exclusively.

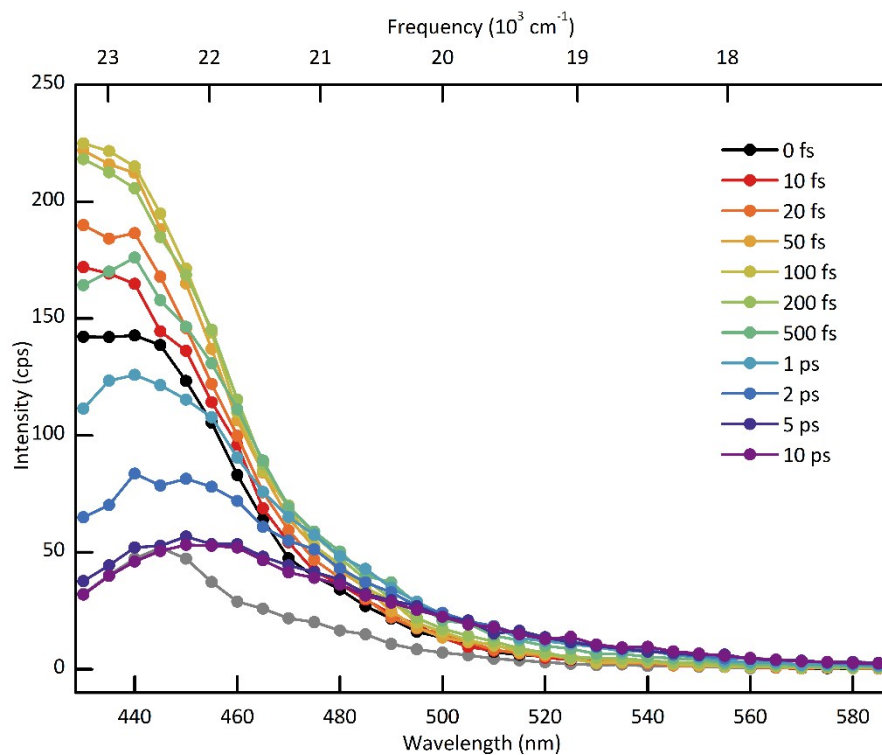


Fig. S5 TF spectra of BA in acetone at the given time delays. In this polar solvent, rise of the long wavelength band is observed as a result of the formation of CT state, as observed for BA in acetone and ethanol.

Global fit of the TF spectra of BA in acetonitrile

One potential problem of using the integrated intensity as the CT dynamics is the spectral shift of the LE state band due to solvation and other relaxation processes. As we cannot integrate entire region of the LE band because of the interference from the Raman scattering, spectral shift of the LE band may affect the total area and introduce some error in the dynamics. To examine the effect of the spectral dynamics of the LE band, global fitting of the TF spectra of BA in acetonitrile has been performed. Some representative fit results are shown in Fig. S8. Nearly the same kinetic information has been obtained from the global fit, and it is concluded that the LE band display negligible spectral dynamics even in polar solvents.

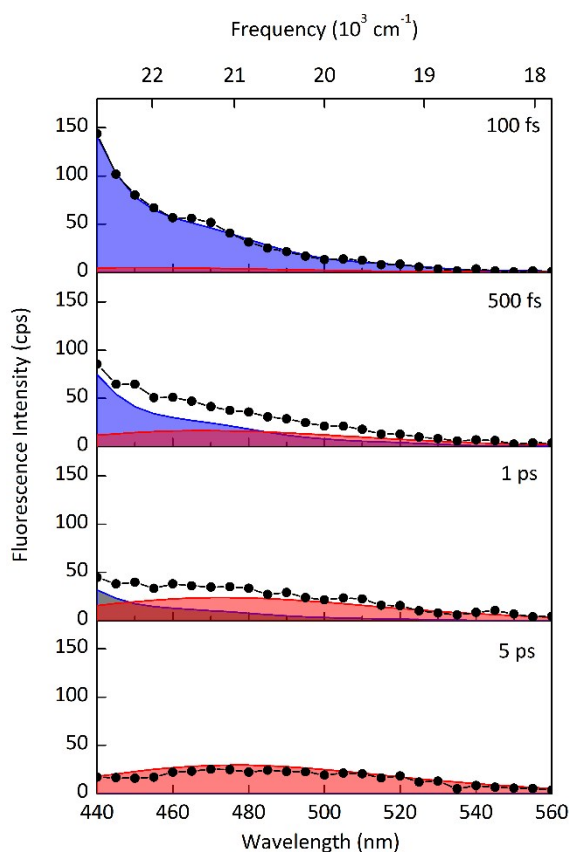


Fig. S6 Global fitting result of the TF spectra of BA in acetonitrile. The black dots represent the experimental data, and the blue and red shaded areas represent the LE and CT bands, respectively. The TF spectra were fitted globally to two functions representing the LE and CT bands. The LE band was assumed to have the same shape as the TF spectrum at time zero, while spectral shift and amplitude change were allowed during the fit. The CT band was assumed to be a lognormal function with the asymmetry the same as that of the steady spectrum of the CT band in acetonitrile. The spectral shift was assumed to be similar to the solvation function of acetonitrile. Amplitudes of the LE and CT bands were parameterized as a sum of exponential functions. Spectral shift of the LE band was not observed in the global fit, and the kinetics of the CT reaction was determined as the single exponential with the time constant of 597 fs as obtained from the integrated intensity as the CT dynamics.

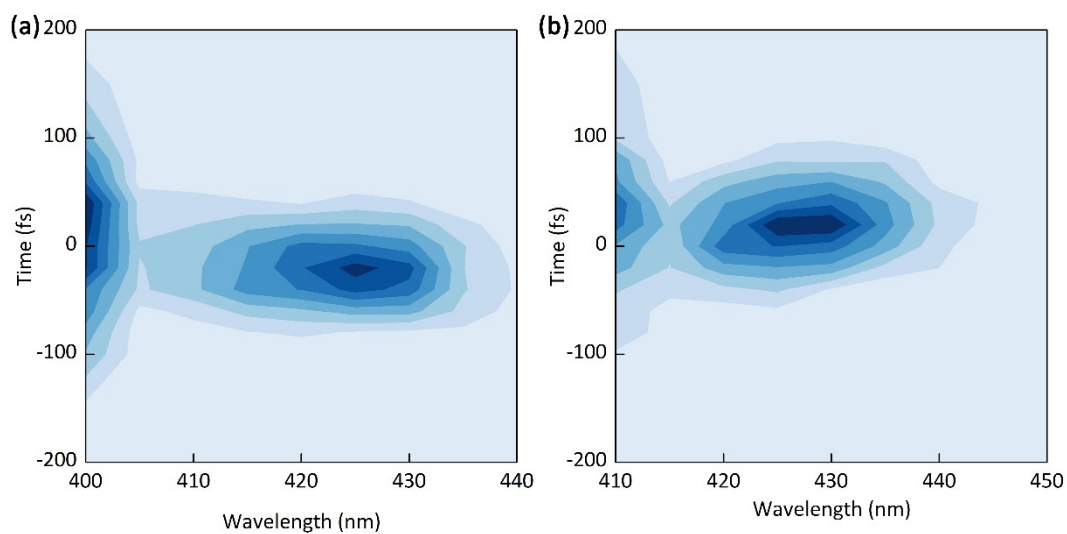


Fig. S7 Time-resolved spectra of pure solvents acetonitrile and ethanol. (a), (b) show the contour plots of the time-resolved spectra of pure solvents acetonitrile and ethanol acquired by exactly the same condition used for the acquisition of the TF spectra of BA. The bands at 425 nm are due to the Raman scattering of the C-H stretching vibrations of solvent molecules. Contribution of the Rayleigh and Stokes Raman scattering to TF spectra of BA can be assessed from these reference spectra. Instrument response function (IRF) and time-zero calibration can also be acquired by the solvent Raman scattering.

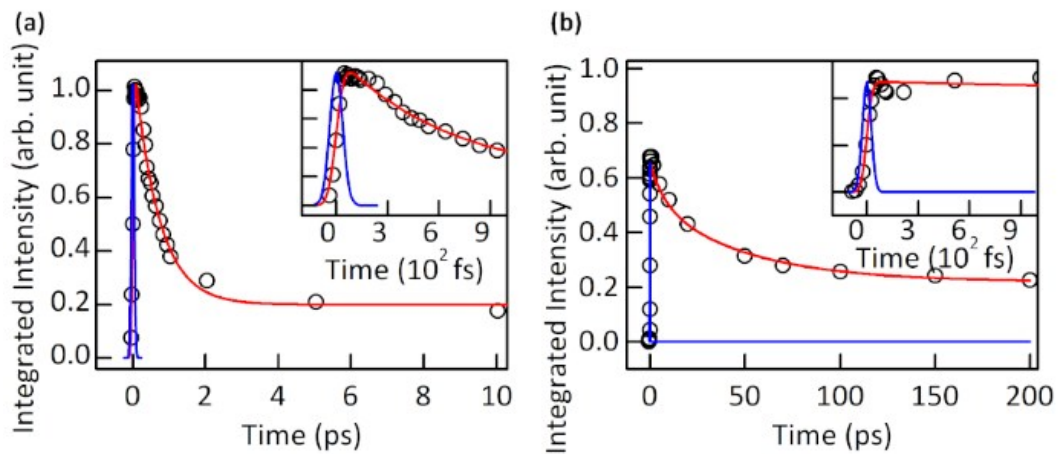


Fig. S8 Integrated area of the whole area of TF Spectra shown in Fig. 1 of (a) acetonitrile and (b) ethanol solvents. In acetonitrile, reaction rate is fitted to be 750 fs, and in ethanol, the rate is found to be 7.8 ps and 49 ps.

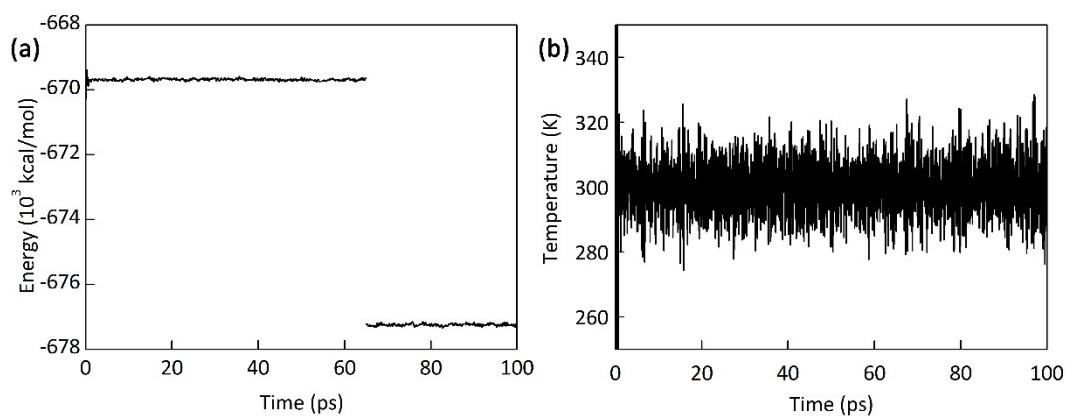


Fig. S9 Equilibration of the ground state in the QM/EFP MD simulation. (a),(b) Total energy and temperature of the MD system that consists of a BA and 378 acetonitrile molecules in a spherical box. Large fluctuations of both energy and temperature can be seen at $t < 1$ ps, and stabilize afterwards. For the calculation of the QM part, Hartree-Fock method with 3-21G basis set was used during the initial 65 ps and DFT method with CAM-B3LYP/6-31G was used afterwards.

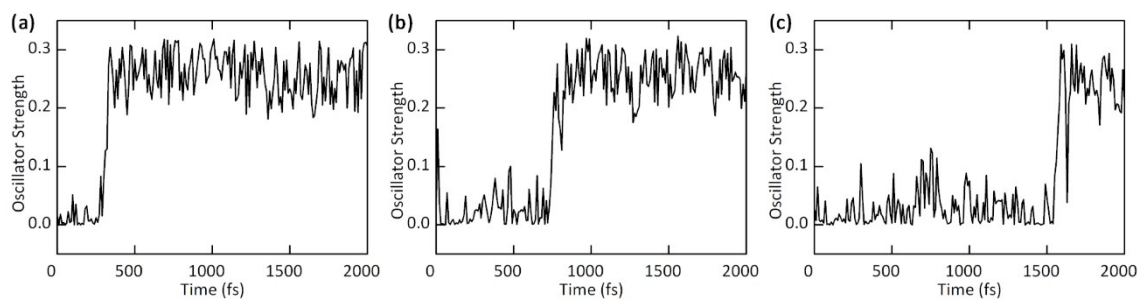


Fig. S10 Oscillator strength of the S_2 state of representative MD simulations. 75% of the MD results (49/65) show similar tendency. 12% of them (8/65) return back to the LE state, and then come back to the CT state, 8% of them (5/65) change slowly, and 5% of them (3/65) do not show the CT reaction.

Occupied Orbital	Virtual Orbital	Excitation Amplitude	De-excitation Amplitude
86	94	0.050	-0.0004
87	94	-0.097	0.0005
93	94	-0.987	0.001
93	100	0.080	0.0004
93	101	0.067	0.00004

Table S1. Transition amplitudes of the S_1 state after CT reaction (2000 fs in Fig. 5 of manuscript). Because this state is the CT state, the main amplitude is shown in $93 \rightarrow 94$ (-0.987), which is the electron transfer from one anthracene ring to another ring as it can be observed in Fig. S11.

Occupied Orbital	Virtual Orbital	Excitation Amplitude	De-excitation Amplitude
92	94	-0.520	0.035
93	95	0.849	-0.066
89	96	-0.049	-0.028
91	97	0.037	0.023
91	98	-0.083	-0.048
87	102	-0.031	-0.030

Table S2. Transition amplitudes of the S_2 state after CT reaction (2000 fs in Fig. 5). Because this state is the LE state, the main amplitude is shown in $92 \rightarrow 94$ (-0.520) and $93 \rightarrow 95$ (0.849), which is local π - π^* excitation as it can be observed in Fig. S11.

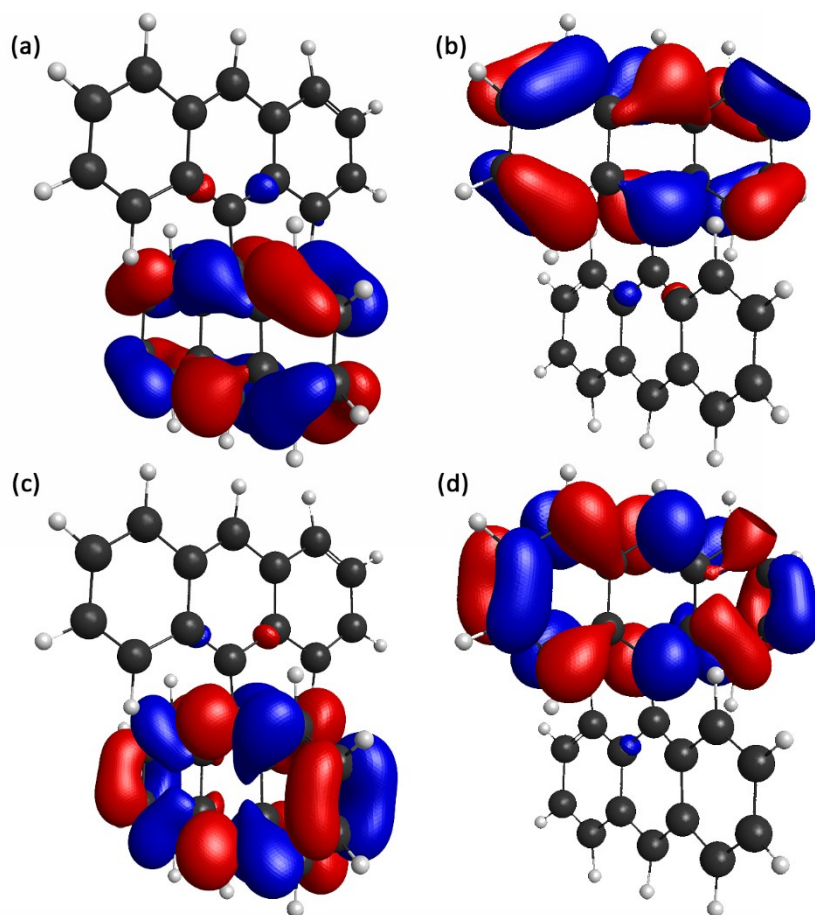


Fig. S11 Molecular orbitals in the MD simulation result (at 2000 fs of Fig. 5 simulation). (a) 92, (b) 93, (c) 94, and (d) 95-th molecular orbitals. 92 and 93 are occupied orbitals and 94 and 95 are virtual orbitals. Transition amplitudes of them are listed in Table S1 and S2.

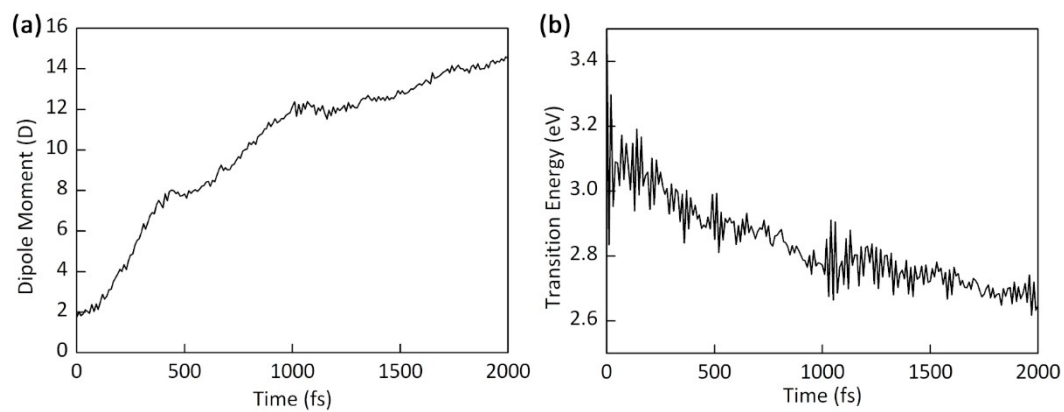


Fig. S12 Ensemble averaged (a) dipole moment of the S_1 state and (b) transition energy between the ground and S_1 states from MD simulations. The change rate is similar to the change of other physical quantities (Fig. 6)

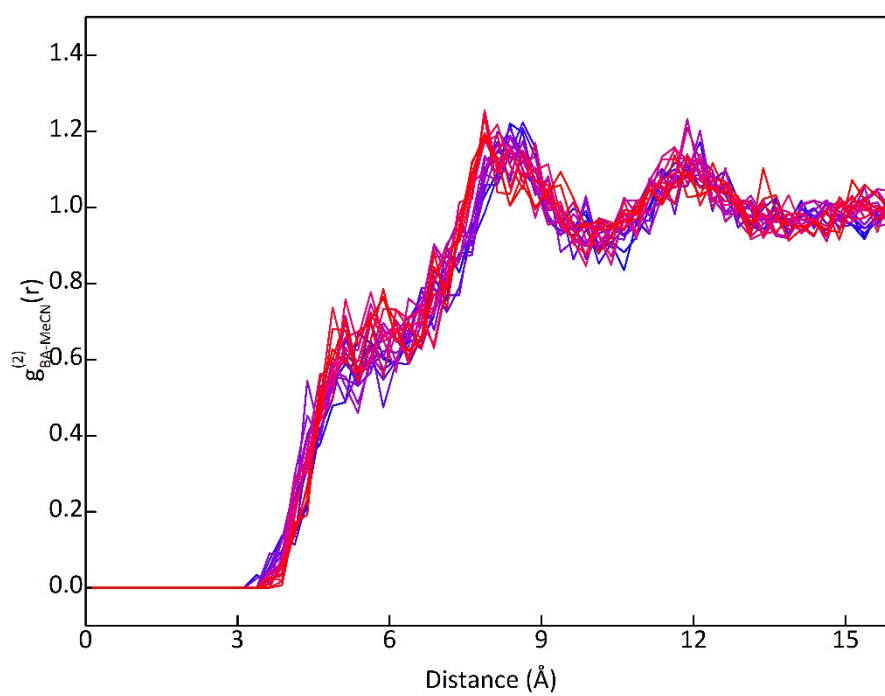


Fig. S13 Radial distribution function (RDF) in the course of MD simulation. RDFs were calculated at every 100 fs from a MD simulation run. Time increases from blue (0 fs) to red (2 ps). No large change of RDF is observed.

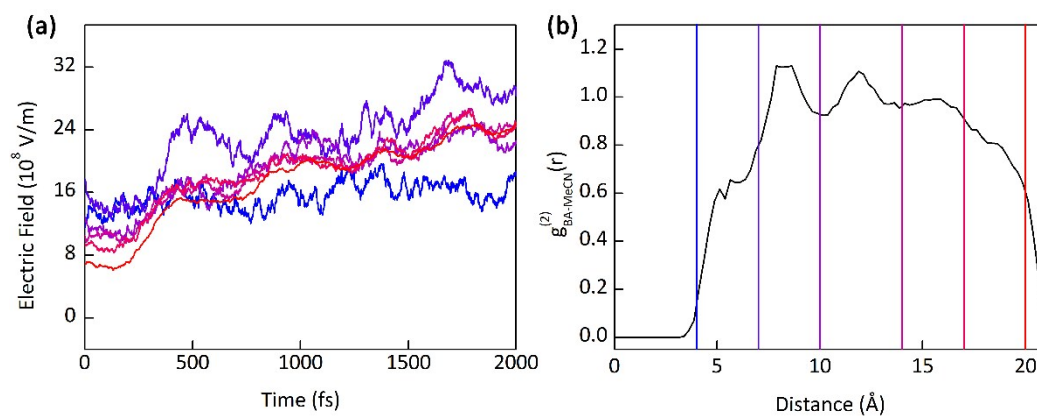


Fig. S14 Spatial distribution of molecules contributing to the electric field. Panel (a) shows the electric field on BA during the MD simulation caused by the acetonitrile molecules within the distance indicated by the color-coded vertical lines in (b). It shows that the first solvation shell within 7 Å makes the major contribution to the electric field. (b) shows the radial distribution function. The vertical lines are placed at 4, 7, 10, 14, 17, and 20 Å.